EPJ Web of Conferences **193**, 01006 (2018) https://doi.org/10.1051/epjconf/201819301006
FISSION 2017

High-statistics reactor anti-neutrino energy spectra for fission and beta-decay studies

Alain Letourneau[1,⋆]

[1] *IRFU, CEA, Université Paris-Saclay, F-91191 Gif-sur-Yvette*

Abstract. With the availability of high-statistics and high-resolution anti-neutrino energy spectra, measured in experiments dedicated to the study of the neutrino oscillation in proximity of a nuclear reactor, we can now envisage to use these data as integral measurements to constrain fission and beta-decay models and nuclear data libraries. In this paper we present the ingredients for the simulation of an anti-neutrino energy spectrum and their sensitivity to the constraint by measured energy spectrum.

1 Introduction

The weak interaction process in nuclei connects two valence orbital states in neutron and proton shells. For light fission-fragments with masses lower than 110 the beta-decay is mainly dominated by transitions between $1g7/2$ neutron orbital and $1g9/2$ proton orbital. For masses above 130 it is dominated by transitions between the $1h9/2$ neutron and the $1h11/2$ proton orbitals. Thus for fission fragments, beta-decays mainly involve transitions between spin-orbit partners with no parity change resulting in strong contributions of allowed Gamow-Teller transitions. However, as shown in figure 1, the contribution of first forbidden transitions with parity change, mainly $0^- \rightarrow 0^+$, are favoured for some nuclei and dominate the high energy part of the lepton (electron and antineutrino) spectrum. The nuclear structure of the daughter nuclei strongly influence the energy spectrum of the lepton-emitted particles. Measuring the characteristics (shape and end-point) of these particles should give insight on the structure of the daughter nuclei and on the beta-decay process itself.

Measuring the electron-energy spectra for selected nuclei is the easiest and most convenient way. Unfortunately it faces two major problems. The first one is that it requires a high-resolution electron spectrometer, as the BILL spectrometer [1] running at ILL in the 80's, with large dynamic to cover the full energy range of very neutron-rich nuclei (up to 8 MeV). The second one is that the electron-energy spectrum suffers from corrections due to electromagnetic perturbations in the nucleus, the atom and the target. Another approach would be to use the antineutrino-energy spectrum measured for selected nuclei but due to the weak neutrino interaction cross section, large volume detectors and highly radioactive targets are needed, limiting to few nuclei with long half-lives as ^{144}Ce-^{144}Pr [2], ^{51}Cr [3] and ^{37}Ar [4]. Antineutrino-energy spectra measured in reactor anti-neutrino experiments could be another alternative to put constraints on beta-decay and fission models and nuclear data libraries. Indeed, anti-neutrinos are produced during the beta-decay chain of the fission fragments. The energy spectrum then results from the contribution of each individual beta-decay transitions and

⋆e-mail: aletourneau@cea.fr

the fission fragment production which depends on the fissioning system. Even if this method is less selective it offers the advantage of an integral measurement with an electromagnetically-unperturbed probe.

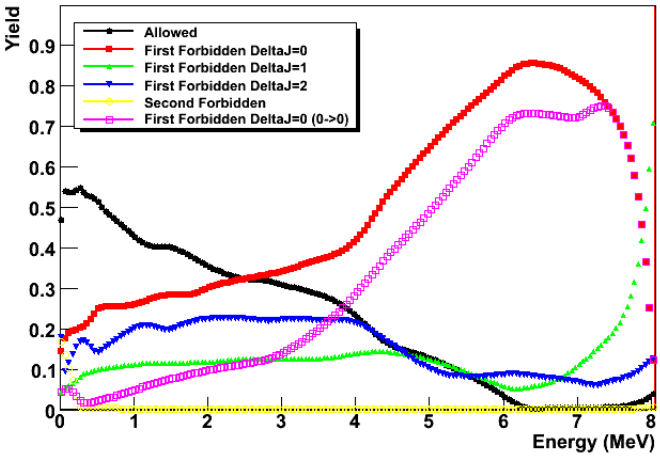

Figure 1. Contributions of different transition types determined from the ENSDF data base [22] in the electron-energy spectrum calculated for the fission of ^{235}U induced by thermal neutrons.

In the last years, several reactor anti-neutrino experiments have been launched to measure the propagation properties of the electronic anti-neutrino at short distance (less than 1 km). Some of these experiments with large volume detectors have already provided the community with high-statistics and high-resolution anti-neutrino energy spectra [5–7]. Other experiments [8–14] will provide in a close future energy spectra with unprecedented quality and statistics. If most of them will provide energy spectra for a mixing of different fissioning systems, some of them as the Stereo experiment at ILL [9] will provide an energy spectra for the pure fission of ^{235}U.

In this paper, we discuss the ingredients used to model the reactor antineutrino-energy spectra and their sensitivity on the energy spectra.

2 Lepton-energy spectra for a fissioning system

2.1 Beta-decay spectrum for a single transition

In the Fermi theory of beta-decay, the energy spectrum for an electron (or an anti-neutrino) emitted with a kinetic energy E_e (E_ν), is expressed as:

$$P(E_e)dE_e = C_{\Delta J^\pi}(Z, E_e)P_0(E_e)F(Z, E_e)\delta(Z, A, E_e)dE_e \tag{1}$$

The phase-space factor $P_0(E_e)$ is expressed as a function of the electron momentum (p_e) and the total energy of the transition (E_0) as:

$$P_0(E_e) = \frac{G_F^2}{2\pi^3} p_e E_e (E_0 - E_e)^2 \tag{2}$$

Using the energy sharing between the two leptons $E_0 = E_e + E_\nu$ (neglecting the recoil of the nucleus), the probability to emit an anti-neutrino with total energy E_ν can be expressed in a similar way than Eq.1. $F(Z, E_e)$ is the Fermi function needed to account for the deceleration of the electron in the Coulomb field of the nucleus with Z protons. The Fermi function is calculated for a point-like charge and the correction term $\delta(Z, A, E_e) = 1 + \delta_{FS} + \delta_{rad} + \delta_{WM}$ is added as in [15] to account for the finite size of the nucleus (δ_{FS}), the weak current induced by the interference of the magnetic moment distribution of the vector current with the spin distribution of the axial current (δ_{WM}) and the exchange of real and virtual photons between the electron and the nucleus (δ_{rad}). In this work we used the expression derived by Sirlin [16] for the radiative term $\delta_{rad}(Z, A, E_e)$, and the expressions derived by Hayes et al. [17] for the finite size term $\delta_{FS}(Z, A, E_e)$ and the weak magnetism term $\delta_{WM}(Z, A, E_e)$.

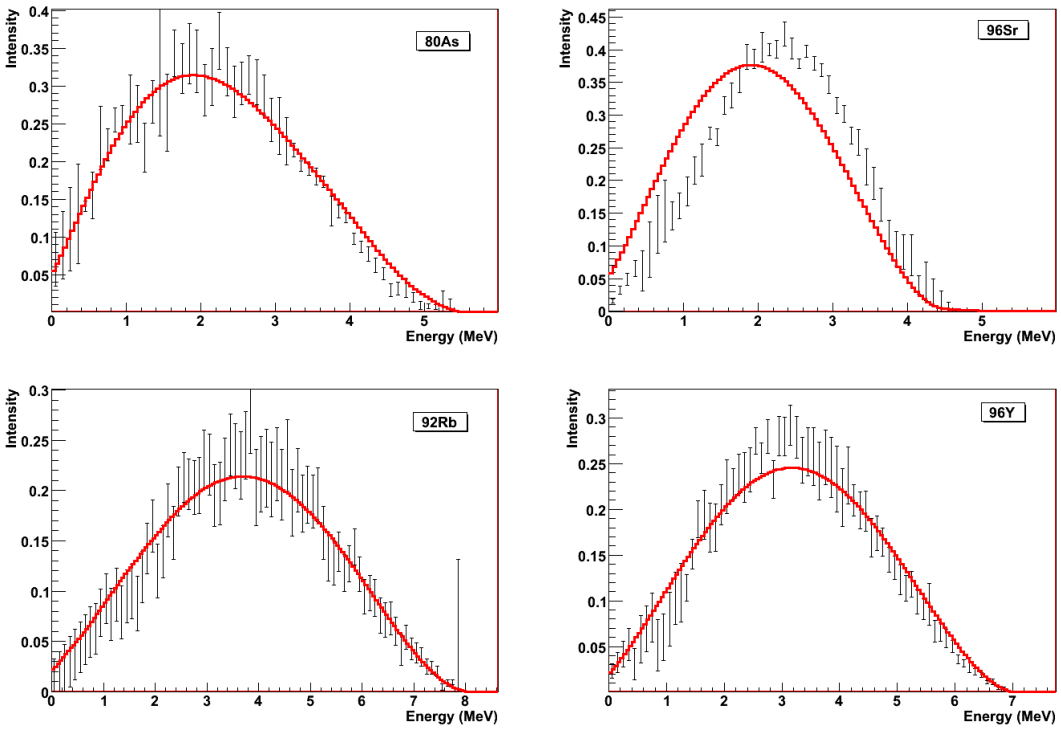

Figure 2. Examples of calculated energy spectra for almost pure allowed transitions (^{80}As, ^{96}Sr) and dominant non-unique first-forbidden transitions (^{92}Rb, ^{98}Y) compared with the Rudstam data [23].

The shape factor $C_{\Delta J^\pi}(Z, E_e)$ contains the nuclear transition-matrix elements and the energy dependance of the wave functions for the electron and the anti-neutrino. The ΔJ^π-index refers to the spin and parity changes between the initial and final nuclear states of the transition. The shape factors for allowed, first and second forbidden transitions were originally derived by Konopinski and Uhlenbeck [18]. In their derivation they evaluated the radial wave function of the electron and the neutrino by solving the Dirac equation at the nuclear radius for a point-like nuclear charge. This approximation is a crude approximation that could lead to uncertainties but which offers the possibility to take out the energy dependence of the leptons radial wave functions from the nuclear matrix elements. The

lepton and nuclear transition matrix elements can then be treated separately. An exact treatment of the lepton radial wave functions and the expressions to calculate exactly the shape factors were proposed by Buhring [19]. In these expressions, lepton and nuclear transition matrices could not be separated anymore and the hamiltonian should be solved taking into account the lepton wave functions and the nucleons wave functions inside the nucleus. Nuclear models are then needed to calculate the nucleons wave functions inside the nucleus. Generally these calculations are highly computer consuming, oftenly limited to some nuclei and the precision on the energy of the transition around few hundred of keV.

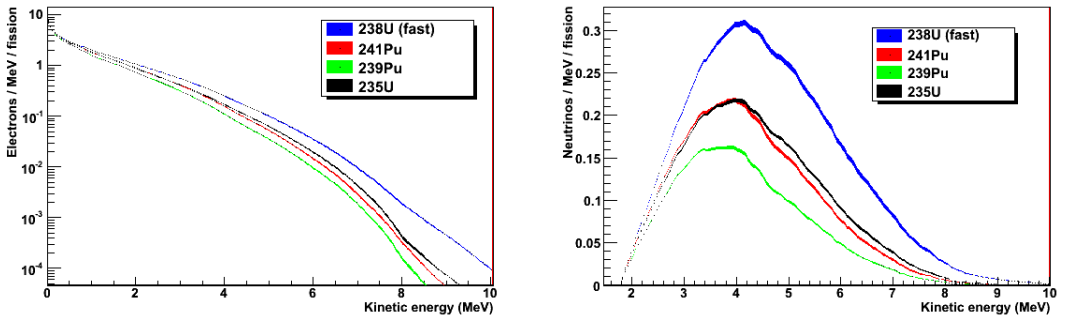

Figure 3. Electron (left) and anti-neutrino (right) energy spectra calculated for different fissioning systems using the cumulative fission yields from JEFF3.1.1 at 25.3 meV for ^{235}U, ^{239}Pu, ^{241}Pu and at 400 keV for ^{238}U. The anti-neutrino energy spectra are convoluted by the inverse beta-decay cross section from [27]. Propagated nuclear data base uncertainties are contained within the width of the histograms.

For all these reasons and for simplicity we decided, in this work, to keep the Konopinski and Uhlenbeck approach. The shape factor $C_{\Delta J^\pi}(Z, E_e)$ for a transition is then expressed as a linear combination of the electron and antineutrino kinetic terms weighted by the nuclear transition-matrix elements, the latter being treated as free parameters keeping the selection rules of the vectorial and axial operators. In the case of allowed transitions with no parity change ($\Delta J = 0, 1$), the shape factor is constant and the shape of the anti-neutino spectra reduces to the phase-space shape corrected from the coulomb effects. In the case of first-unique forbidden transitions with parity change ($\Delta J = 2$), only one matrix element contributes and the shape factor could be reduced to a polynomial function of the electron momentum. For non-unique forbidden transitions, with general considerations it is possible to relate nuclear matrix elements each others. Such approach was done by Ahrens and Feenberg [20] where from general physical arguments as the conservation of the vector current they derived linear relations between momentum type and coordinate type nuclear matrix elements for the vectorial operators. Similar relation was also derived between the vectorial and axial matrix elements in the single particle model [21]. We do not detail too much here but details and expressions can be found in reference [21]. Using these relations, the nuclear matrix elements reduce to one parameter for the vectorial term and one for the axial term that we treated as random variables varying within the experimental values quoted in [21].

Ingredients for the calculations as end-point energy, spins and parities of the initial and final states are taken from ENSDF nuclear structure data base [22] and uncertainties on the values or spin and parity assignements are propagated by Monte-Carlo method. When the spin and/or the parity of the daughter level are not known, the logft value is used to decide the type of the transition. Very few

electron-energy measurements exist for nuclei in the fission-fragment region but an extensive campaign of measurements on short-lived fission fragments was done by Rudstam et al. [23]. Examples of comparison of the calculated spectra with the measured electron-energies are shown on figure 2 for two selected almost pure allowed transitions (^{80}As, ^{96}Sr) and for two dominant $0^- \rightarrow 0^+$ to the ground state non-unique first-forbidden transitions (^{92}Rb, ^{98}Y). As seen on the figure, ^{80}As and ^{92}Rb are quite well reproduced, validating the calculations whereas there is a clear discrepancy on ^{96}Sr pointing either a problem in the measurement or in the ENSDF nuclear data base. A more systematic study on all the data measured by Rudstam et al. draws the same conclusion of an overall good agreement for some nuclei and large inconsistencies for others questioning the quality of the data for these nuclei or the quality of the ENSDF data. In this work we do not investigate further these discrepancies but seeing the large uncertainties for some measurements, new high quality measurements are required to better constraint the shape of the electron energy spectra for fission-fragment isotopes but also to test the consistency with the ENSDF nuclear structure data library.

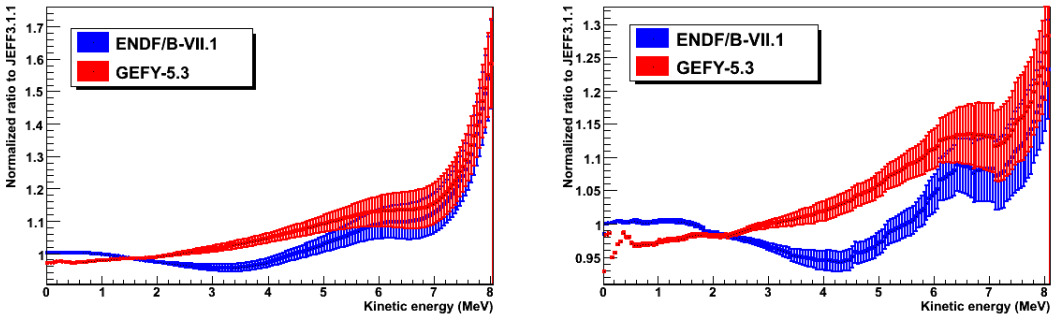

Figure 4. Normalized ratio of the calculated energy spectra for ^{235}U using cumulative fission yields from ENDF/B-VII.1 and GEFY-5.3 to the calculated spectra using JEFF3.1.1 for electrons (left) and anti-neutrinos (right). The uncertainties are propagated nuclear data bases uncertainties.

2.2 Beta-decay spectrum for a fissioning system

The lepton energy spectrum for a fissioning system is calculated by summing over all the beta-decay branches of a fission fragment weighted by its activity which depends on the fission yield but also on its time evolution due to its decay, its feeding by parents and to the neutron captures. For pulse fission, independent fission yields can be used but for longer-time irradiations, evolution codes have to be used to estimate the time-evolution of the fragments. In the following, we used cumulative fission yields considering long irradiation times with fragments in equilibrium.

The calculated electron and anti-neutrino energy spectra for different fissioning systems are shown on figure 3 using the cumulative fission yields from JEFF3.1.1 nuclear data library [24]. The anti-neutrino energy spectra are convoluted by the inverse beta-decay cross section, the reaction used to detect anti-neutrinos. Due to unknown level scheme for some nuclei about 10% of the energy spectra could not be modeled as already pointed out in [15]. In that previous work, fictive level schemes were introduced to complete the missing schemes but we do not retain this solution in that work.

As seen on the figures, the shapes and the integrals depend on the fissioning system. As discussed in [28] the dependence is mainly due to light fission-fragments and specifically odd-Z and odd-N

nuclei having large Q_β values and low-spin ground-state feeding directly the ground state of the even-even daughter. This effect is much visible in the high energy-part of the spectrum where anti-neutrinos are the most sensitive due to the increasing cross-section of the beta inverse process as a function of the anti-neutrino energy.

This feature is at the origin of the idea to use anti-neutrinos as non-intrusive probe to monitor the operational status of a nuclear reactor (see for example [30]). Indeed, as ^{239}Pu emits less anti-neutrinos than ^{235}U, the two major contributors to the fission power in a comercial PWR, the number of anti-neutrinos reduces as one goes along the burn-up increases as observed in the different neutrino experiments [5, 6, 8].

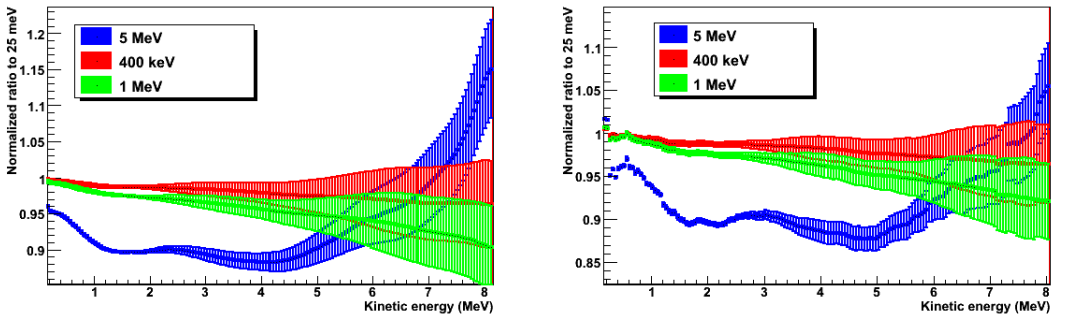

Figure 5. Normalized ratio of the calculated energy spectra for ^{235}U using 500 keV, 1 MeV and 5 MeV incident neutron cumulative fission yields from GEFY-5.3 to the energy spectra using the 25.3 meV fission yields for electrons (left) and anti-neutrinos (right). The uncertainties are propagated from nuclear data bases.

3 Sensitivity study

In the following we present the impact of different ingredients of the modelisation onto the electron and anti-neutrino energy spectra.

3.1 Sensitivity to fission yields

First of all we start with the impact of the fission yields. Figures 4 shows the normalized ratio of the calculated electron and anti-neutrino energy spectra associated to the ^{235}U thermal fission, using cumulative fission yields from ENDF/B-VII.1 nuclear data library [25] and the GEF code version 5.3 [26] electron to the JEFF3.1.1. A quiet good agreement is observed below 2 MeV but discrepancies accounting for more than 5 % above 2 MeV and even higher than 10% above 5 MeV for GEFY-5.3 are observed. Such deviation between ENDF/B-VII.1 and JEFF3.1.1 was already pointed out in [29] finding the origin into anomalous fission yields for some isotopes in ENDF/B-VII.1 that should be corrected into the latest ENDF release.

The dependence with the energy of the incident neutron inducing the fission is shown on figure 5 using the GEFY-5.3 by comparing the cumulative fission yields at 25.3 meV, 400 keV, 1 MeV and 5 MeV in ^{235}U fission. We see a small evolution of the electron and anti-neutrino energy spectra when the excitation energy of the fissioning system is below few MeV above the fission barrier but strong variations of about 10 % appear when increasing the excitation energy. This is due to the vanishing

effect of nuclear structure resulting in less pronouced odd-even effect in the fission fragments and an increase of symmetric fission.

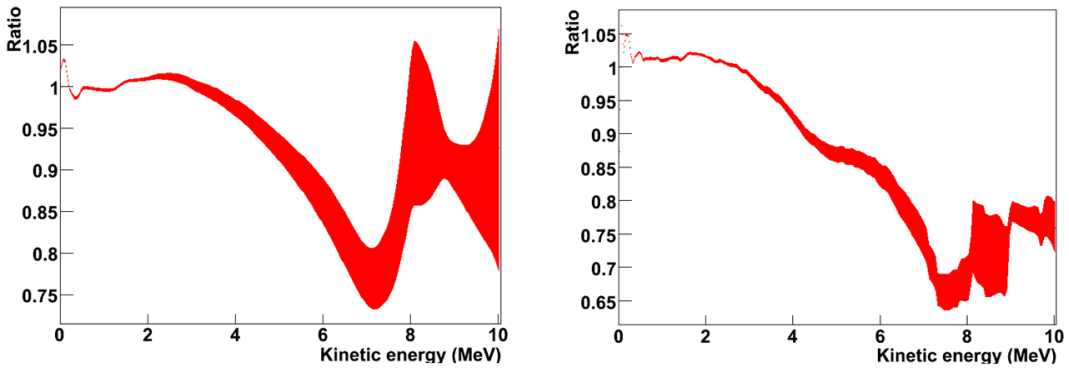

Figure 6. Normalized ratio of the calculated electron (left) and anti-neutrino (right) energy spectra when transitions are treated according to their type to the spectra when transitions are treated as allowed. Only uncertainties on spin-parity assignement in ENSDF have been propagated.

3.2 Sensitivity to transition modelisation

The impact of treating transitions according to their type in particular for non-unique first forbidden transitions is shown on figures 6 where the electron and antineutrino energy spectra are compared to the case where all transitions are treated as allowed transitions. Large variations are observed above 2-3 MeV showing the sensitivity of electron and antineutrino energy spectra to constraint the nuclear matrix elements for first-forbidden transitions, particularly for $0^- \rightarrow 0^+$ transitions.

4 Conclusion

In this paper we have shown the potentialities of high-statistics and high-resolution anti-neutrino energy spectra measured in reactor anti-neutrino experiments. We have shown that they could be used as integral measurements to check the consistency and constraint the fission yields from nuclear data bases or fission models, and to validate the modelisation of the lepton energy spectra based on nuclear structure-data library. Due to the beta-inverse reaction, anti-neutrinos are mainly sensitive to the high energy part of the spectrum where very few isotopes contribute with strong $0^- \rightarrow 0^+$ transitions to the ground state. Coupled with new and high-quality electron energy measurements for these isotopes, the modelisation presented in this paper could be used to extract nuclear matrix elements giving insight onto the nuclear structure of the daughters.

Daya-Bay and NEOS experiments have already provided high quality anti-neutrino energy spectra but for a mixed contain of fissile isotopes. Soon, with the Stereo experiment, a pure ^{235}U anti-neutrino energy spectra will be available complementing the electron energy spectra measured at ILL [31]. A combined analysis on these two set of data will be conducted to extract new information on the beta-decay modelisation. In return, a better knowledge of the weak process in the nuclei will be helpfull for future neutrino experiments, for r-process nucleosynthesis and to test the standard model in the beta-decay of nuclei.

References

[1] W. Mampe *et al.*, Nucl. Inst. Meth. **154**, 127 (1978).
[2] M. Cribier *et al.*, Phys. Rev. Lett. **107**, 201801 (2011); J. Gaffiot et al., Phys Rev. D**91**, 072005 (2015).
[3] J.N. Bahcall, P.I. Krastev, E. Lisi, Phys. Lett. B **348**, 121 (1995); J. N. Abdurashitov et al., Phys. Rev. C **59**, 2246 (1999).
[4] J. N. Abdurashitov *et al.*, Phys. Rev. C **73**, 045805 (2006).
[5] F.P. An *et al.* (Daya Bay collaboration), Chinese Physics C**41**, 013002 (2017).
[6] J.K. Ahn *et al.* (RENO collaboration), PL 108,191802 (2012); arXiv:1610.04326v3 (2017).
[7] Y.J. Ko *et al.* (NEOS collaboration), Phys. Rev. Lett. **118**, 121802 (2017).
[8] Y. Abe *et al.* (Double Chooz collaboration), JHEP 01, 163 (2016).
[9] A. Bonhomme *et al.* (Stereo collaboration), in Proceedings ot 52nd Rencontres de Moriond, EW Interactions and Unified Theories, La Thuile, March 18-25 (2017); V. Helaine *et al*. (Stereo collaboration), in Proceedings of the Neutrino-2016 conference, arXiv:1610.00003 (2016).
[10] C. Lane *et al.*, arXiv:1501.06935 (2015).
[11] A. P. Serebrov *et al.*, arXiv:1702.00941 (2017).
[12] I. Alekseev *et al.*, arXiv:1606.02896 (2016).
[13] Y. Abreu *et al.*, arXiv:1703.01683v2 (2017).
[14] Z. Djurcic *et al.*, arXiv:1309.7647v3 (2015).
[15] T.A. Muller *et al.*, Phys Rev C**83**, 054615 (2011).
[16] A. Sirlin, Phys. Rev. **164**, 1767 (1967).
[17] A.C. Hayes *et al.*, Phys. Rev. Letters **112**, 202501 (2014).
[18] E.J. Konopinski and G.E. Uhlenbeck, Phys. Rev. **60**, 308 (1941).
[19] W. Buhring, Nucl. Phys. **40**, 472 (1963); W. Buhring, Nucl. Phys. **49**, 190 (1963), W. Buhring, Nucl. Phys. **61**, 110 (1963); H. Behrens and W. Buhring, Nuc. Phys. A**162**, 111 (1971); H. Behrens and W. Buhring, Nuc. Phys. A**150**, 481 (1970).
[20] T. Ahrens and E. Feenberg, Phys. Rev. **86**, 64 (1952).
[21] H. F. Schopper, *Weak interactions and nuclear beta decay*, North-Holland Publishing Company, 1966.
[22] See http://www.nndc.bnl.gov/ensdf.
[23] G. Rudstam *et al.*, At. Data Nucl. Data Tables **45**, 239 (1990).
[24] M.A. Kellet, O. Bersillon and R. W. Mills, JEFF Report 20, NEA, OECD, 2009.
[25] M.B. Chadwick *et al.*, Nucl. Data Sheets **112**, 2887 (2011).
[26] K.-H. Schmidt, B. Jurado, Ch. Amouroux, Ch. Schmitt, Nucl. Data Sheets **131,** 107 (2016); See also http://www.cenbg.in2p3.fr/GEF.
[27] A.M. Ankowski, arXiv:1601.06169v1 (2016).
[28] A.A. Sonzogni, T.D. Johnson and E. A. McCutchan, Phys. Rev. C**91**, 011301(R) (2015).
[29] A.A. Sonzogni *et al.*, Phys. Rev Lett. **116**, 132502 (2016).
[30] G. Boireau *et al.* (Nucifer collaboration), Phys. Rev. D**93**, 112006 (2016).
[31] K. Schreckenbach *et al.*, Phys. Letters B**99**, 251 (1981); K. Schreckenbach *et al.*, Phys. Letters B**160**, 325 (1985).